HAL
archives-ouvertes.fr

Magnetic behavior of exchange-coupled Fe 30 Au 70 / Fe 65 Au 35 bilayers

F. Canet, C. Bellouard, L. Joly, S. Mangin

▶ **To cite this version:**

F. Canet, C. Bellouard, L. Joly, S. Mangin. Magnetic behavior of exchange-coupled Fe 30 Au 70 / Fe 65 Au 35 bilayers. Physical Review B : Condensed matter and materials physics, American Physical Society, 2004, 69 (9), pp.094402. 10.1103/PhysRevB.69.094402 . hal-02086060

HAL Id: hal-02086060
https://hal.univ-lorraine.fr/hal-02086060

Submitted on 1 Apr 2019

HAL is a multi-disciplinary open access archive for the deposit and dissemination of scientific research documents, whether they are published or not. The documents may come from teaching and research institutions in France or abroad, or from public or private research centers.

L'archive ouverte pluridisciplinaire **HAL**, est destinée au dépôt et à la diffusion de documents scientifiques de niveau recherche, publiés ou non, émanant des établissements d'enseignement et de recherche français ou étrangers, des laboratoires publics ou privés.

Magnetic behavior of exchange-coupled $Fe_{30}Au_{70}/Fe_{65}Au_{35}$ bilayers

F. Canet, C. Bellouard, L. Joly, and S. Mangin*
Laboratoire de Physique des Matériaux (UMR CNRS 7556), Université Henri Poicaré, BP 239, F-54506 Vandoeuvre-Lés-Nancy cedex, France

(Received 16 May 2003; revised manuscript received 30 October 2003; published 9 March 2004)

The evolution of magnetic configurations inside ferromagnetic $Fe_{30}Au_{70}/Fe_{65}Au_{35}$ bilayers have been studied. The two FeAu alloys magnetization are ferromagnetically exchange coupled at the interface and both exhibit an in-plane uniaxial anisotropy. The magnetization reversal of a bilayer from one saturated state to the other occurs via an interface domain wall state, which is metastable. This interface magnetic domain wall which spreads mainly in the soft $Fe_{30}Au_{70}$ layer is pinned at the interface by the harder $Fe_{65}Au_{35}$ alloy. Its presence and its ''compression'' are evidenced by magnetization, electrical transport, and ac-susceptibility measurements combined with a unidimensional micromagnetic calculation. In order to investigate magnetization reversal dynamics, temperature dependence as well as magnetic aftereffect measurements were performed. The magnetization reversal process is found to be thermally activated and activation parameters could be deduced.

DOI: 10.1103/PhysRevB.69.094402 PACS number(s): 75.60.Jk, 75.70.−i, 75.60.Lr

I. INTRODUCTION

The exchange coupling between magnetic layers is currently of interest for theoretical and technical reasons. It is studied in a large variety of systems which combine ferromagnetic, ferrimagnetic, or antiferromagnetic layers which can be magnetically hard or soft and whose structures are single crystalline, polycrystalline, or amorphous.[1–3]

In a lot of systems, the interface magnetic interaction results in a shift of the hysteresis loop described through a so-called exchange bias field H_E. Such phenomena are typically observed in ferromagnetic and antiferromagnetic systems[4–6] and soft and hard ''spring magnet'' systems.[3,4,7–12] According to the net magnetization of the materials and the sign of the interface interaction, positive or negative shifts of the magnetic loop occur.[13–15] These effects are now used in spin-electronic devices[16,17] based on giant magnetoresistance effects or tunnel magnetoresistance effects and in which it turns out to be of great interest to control the reversal field of one of the layer magnetization and to shift this field from zero.

Beyond macroscopic descriptions, it is of interest to understand microscopic mechanisms, which lead to exchange bias phenomena. Some models are based on the presence of a domain wall at the interface between a first material, whose magnetization is poorly sensitive to the field (because its net magnetization is zero or because it is quenched along an easy magnetic axis), and a second one, magnetically coupled to the first one, whose magnetization easily follows the field. Such a model seems to be valid for magnetically hard and soft spring magnet bilayer systems,[18] which are still under heavy discussions in antiferromagnetic and soft ferromagnetic materials in which this concept was introduced by Mauri *et al.*[19] In that case the domain wall would play a central role in the magnetic reversal processes of the system.[20–22]

In previous papers, we have reported results of studies performed on the amorphous GdFe/TbFe system in which TbFe is a very hard ferrimagnetic alloy and GdFe is a soft ferrimagnetic material.[3,18] In this system, a uniaxial anisotropy axis was created by using anisotropic evaporation conditions for GdFe (Ref. 23) and by field cooling for TbFe. From various measurements, we could deduce that the reversal of the magnetic field led first to a reversal of the magnetization in GdFe, starting from the outer surface of this layer, and we showed that the reversal of the magnetization was stopped against the TbFe layer with the formation of an interface domain wall mainly located inside the soft layer (GdFe).[18] Note that those interpretations are generally admitted and confirmed for other ''spring magnet'' systems.[1,9–12] Under the pressure generated by the magnetic field, the domain wall is compressed against the TbFe potential barrier and eventually the magnetic field leads to the reversal of the TbFe layer magnetization when it becomes large enough. Such a system has the particularity to be made of isostructural amorphous materials, which ensures a continuity of the structure at the interface and prevents interface defects that can play an important role in the pinning of the domain wall.

The question is to know in which extent the formation of a domain wall at the interface between magnetic layers is general? What is the role of magnetic parameters such as anisotropy, exchange stiffness at the interface, and magnetization of the two layers? What is the part of the nature of the magnetic material ferromagnet, ferrimagnet, or antiferromagnet? What is the role of the interface structure: we can for example expect that clean interfaces without any defects would lead to well-defined and uniform domain walls and that interface defects are the source of lateral domain formation as in a Malozemoff model like that of Ref. 24.

In this paper, we present a study performed on the $Fe_{30}Au_{70}/Fe_{65}Au_{35}$ bilayer system, which offers some specific characteristics. (i) Both FeAu alloys are ferromagnetic but with significantly different magnetic parameters, which will lead to the occurrence of a moderate potential barrier at the interface between the two alloys. (ii) The two layers are made of the same elements, so $Fe_{30}Au_{70}/Fe_{65}Au_{35}$ will present a kind of interface chemical continuity. (iii) The FeAu alloys are polycrystalline and exhibit different structures.

At first, we will focus on the iron-gold system and the

 ©2004 The American Physical Society

structural and magnetic characteristics of the two components of the bilayers: $Fe_{30}Au_{70}$ and $Fe_{65}Au_{35}$. In Sec. II, we describe the magnetic behavior of samples where a thin gold layer separates the two iron-gold alloys and which reveal the characteristics of the two magnetic layers independently. In Sec. III, we examine the behavior of the magnetically coupled layers and in which extent their interaction acts on the magnetization reversal processes. The thickness dependence of both layers on magnetization reversals is examined both qualitatively and quantitatively using a one-dimensional micromagnetic calculation. In Sec. IV, we focus on the interface domain wall: its contribution to the magnetic ac susceptibility and to the electrical resistivity. Finally in Sec. V, we study the dynamics of the magnetization reversal processes through its thermal dependence and magnetic relaxation measurements and conclude on the thermal activation parameters of the process.

II. SYSTEM

According to their phase diagram, iron and gold are very few miscible and the equilibrium state are a mixture of two phases: a fcc phase very rich in gold and a bcc one very rich in iron. However, as has been shown by Mader *et al.*,[25] because of the large difference between the atomic sizes of the two elements, the vacuum codeposition of iron and gold atoms on a cold substrate can lead to the formation of amorphous ''homogeneous'' alloys or to very small crystallites. As shown by Marchal *et al.*[26,27] the thin Fe_xAu_{1-x} films obtained by codeposition of the elements on a substrate kept at the liquid nitrogen temperature are found to be amorphous if $x>0.6$. This phase is, however, poorly stable and the films crystallize in a bcc phase below room temperature by forming very broad grains (1 μm diameter) exhibiting a [110] texture. According to the same authors, the deposited phase is not amorphous anymore when $x<0.6$, but is made of tiny fcc grains, which are still homogeneous at room temperature.

So we focused on the $Fe_{30}Au_{70}/Fe_{65}Au_{35}$ bilayered system prepared by high-vacuum coevaporation on glass substrates kept at liquid nitrogen temperature during the deposition process and subsequently heated to room temperature. By performing transmission electron microscopy at room temperature, we have confirmed previous results[26,27] and observed randomly oriented 20-nm fcc grains for $Fe_{30}Au_{70}$ layers and 1-μm-size bcc grains diffraction pattern for $Fe_{65}Au_{35}$ films. We could in addition evaluate the lattice parameters of these two phases: $a=0.385$ nm for the fcc structure and 0.285 nm for the bcc one. Finally, a coupled x-ray analysis has confirmed the composition of the alloys.

Then arises the question of the occurrence of a single in plane anisotropy axis which is required to provide a ''model system'' to study magnetization reversal. This anisotropy axis was observed in amorphous materials such as GdFe prepared in similar geometry conditions.[23] As shown in Fig. 1, the 100-nm $Fe_{30}Au_{70}$ alloy layer exhibits a clear uniaxial anisotropy axis at $T=300$ K. When the magnetic field is applied perpendicularly to the easy magnetic axis, the magnetization decreases linearly with the field between $-H_K$ and $+H_K$ as predicted by the Stoner-Wohlfart model[28] and a square hysteresis loop (with a coercive field H_C) is observed for a magnetic field applied parallel to the easy direction. As for the GdFe system,[23] the easy axis lies in the plane of the film and is perpendicular to the direction defined by the iron and gold crucibles. At this temperature, the coercive field H_C is very small. H_C is, however, larger and an opening of the hysteresis loop along the hard axis is observed at low temperature; still, H_C and H_K are reasonably well defined. The thermal dependence of H_C, H_K, the measured saturation magnetization M_S, and the anisotropy constant K given by $K=(H_K M_S)/2$ are shown in Fig. 2. Both M_S and K de-

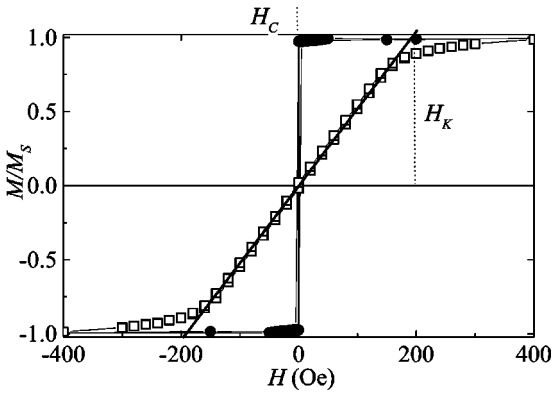

FIG. 1. Normalized magnetization (M/M_S) hysteresis loop obtained on a 100-nm-thick $Fe_{30}Au_{70}$ alloy layer at 300 K for a field H applied along the easy axis (solid circle) and along the hard axis (open square). H_C the coercive field along the easy axis and H_K the anisotropy field are defined.

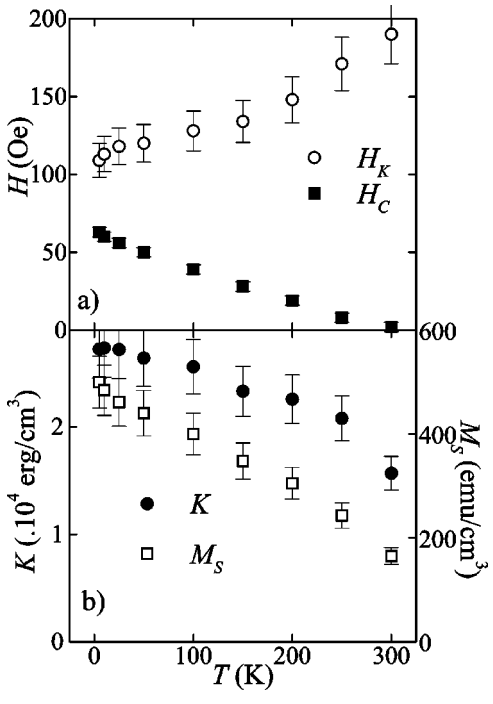

FIG. 2. Temperature (T) dependence on a 100-nm $Fe_{30}Au_{70}$ alloy layer of (a) H_C, the coercive field along the easy axis (solid square), and H_K, the anisotropy field (open circle), and (b) M_S, the measured saturation magnetization (open square), and the anisotropy constant K (solid circle).

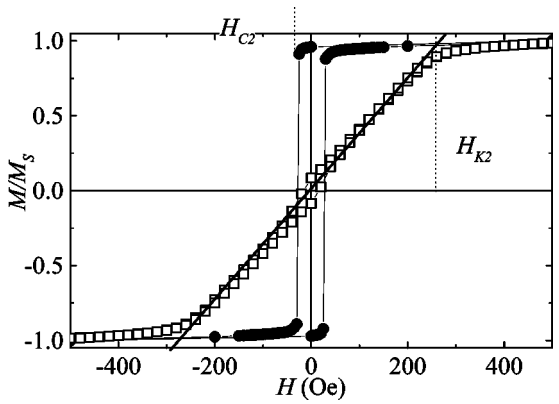

FIG. 3. Normalized magnetization (M/M_S) hysteresis loop obtained on a $Fe_{30}Au_{70}$ (100 nm)/$Fe_{65}Au_{35}$ (100 nm) alloy layer at 400 K for a field H applied along the easy axis (solid circle) and along the hard axis (open square). H_{C2} the coercive field along the easy axis and H_{K2} the anisotropy field are defined.

crease as the temperature approaches the Curie temperature T_C. T_C can be evaluated to 350 K, which is in agreement with the data obtained by Sarkassian.[29] Note that H_C, H_K, and M_S were not found to depend on the layer thickness for thickness ranging from 50 nm to 150 nm.

The $Fe_{65}Au_{35}$ bcc layers deposited on the glass substrates exhibit a poor anisotropy even at high temperature. The growth process and crystallization in kind of spherolites probably rule out memory of the deposition process. However, it appears that $Fe_{65}Au_{35}$ films grown on a previously deposited $Fe_{30}Au_{70}$ layer behave quite differently and exhibit very clearly, at 400 K, the characteristics of an in-plane anisotropy. This is shown in Fig. 3 which represents the magnetic loops, along and perpendicularly to the easy axis, of a ferromagnetic 50-nm $Fe_{65}Au_{35}$ layer deposited on a 100-nm $Fe_{30}Au_{70}$ layer which is, as a matter of fact, paramagnetic at this temperature.

It is then needful to get the magnetic characteristics of a $Fe_{65}Au_{35}$ deposited on a $Fe_{30}Au_{70}$ alloy. In order to magnetically decouple the layers, a thin pure gold layer was deposited between the two films.

The hysteresis loops obtained by applying the magnetic field along and perpendicularly to the easy magnetic axis of a glass/$Fe_{30}Au_{70}$ (100 nm)/Au (3 nm)/$Fe_{65}Au_{35}$ (50 nm) multilayer are shown in Figs. 4(a) and 4(b), respectively, for $T=10$ K. The first drop of the magnetization at H_{C1} in Fig. 4(a) (field applied along the easy axis) corresponds to the reversal of the magnetization of the entire 100-nm-thick $Fe_{30}Au_{70}$ layer. This was proved by repeating the same experiment on samples with different relative layer thickness and by showing that this step is precisely proportional to the $Fe_{30}Au_{70}$ layer thickness. The second drop at H_{C2} corresponds to the reversal of the magnetization of the 50-nm $Fe_{65}Au_{35}$ layer. In addition, the minor cycle of $Fe_{30}Au_{70}$ is centered on 0, which shows that this layer behaves as if it were alone and is not submitted to any significant coupling from the second layer, which would lead to a shift of the hysteresis loop. The thermal variations of H_{C1} and H_{C2} are shown in Fig. 5(a). It is to notice that for all temperatures,

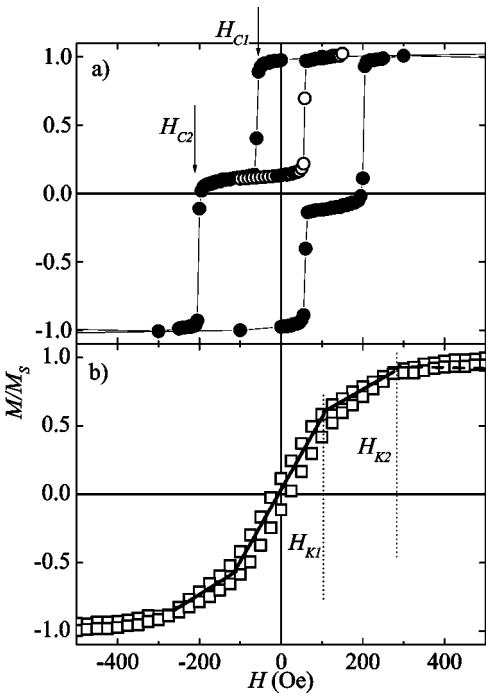

FIG. 4. Normalized magnetization (M/M_S) hysteresis loops obtained on a $Fe_{30}Au_{70}$ (100 nm)/Au (3 nm)/$Fe_{65}Au_{35}$ (50 nm) layer at 10 K (a) for a field H applied along the easy axis and swept from $+2$ kOe to -2 kOe and back to $+2$ kOe (solid circle) and along a minor loop (2 kOe$\rightarrow -100$ Oe$\rightarrow$2 kOe) (open circle) and (b) for a field H applied along the hard axis and swept from $+2$ kOe to -2 kOe and back to $+2$ kOe (open square).

H_{C1} is identical to the coercive field of a single $Fe_{30}Au_{70}$ layer plotted in Fig. 2(a) and that H_{C2} is larger than H_{C1}. The decoupled multilayer has also been measured at 400 K, above the Curie temperature of the $Fe_{30}Au_{70}$ alloy, with an applied field along and perpendicular to the easy axis. The magnetization loops obtained exhibit the same characteristic as the coupled bilayer for $T=400$ K with identical coercive and anisotropy fields. These results allow us to assert that the magnetic characteristics of a 50-nm-thick Fe_{65} Au_{35} layer in a coupled bilayer can be reproduced in a $Fe_{30}Au_{70}$ (100 nm)/Au (3 nm)/$Fe_{65}Au_{35}$ (50 nm) decoupled device.

A typical curve of the magnetization collected at $T=10$ K with the field applied along the direction perpendicular to the easy axis is shown in Fig. 4(b). In that figure, the magnetization versus field curve can be considered as the superposition of two independent linear contributions with their own H_K. The $-H_{K1}$ and $+H_{K1}$ fields for which the net magnetization exhibits a change of slope are for all temperatures very close to the H_K field found on the $Fe_{30}Au_{70}$ single layer in Fig. 2(a). As a consequence, in the decoupled films, H_{K1} is attributed to the $Fe_{30}Au_{70}$ layer and H_{K2} is related to the $Fe_{65}Au_{35}$ layer. Figure 5(b) shows the thermal dependence of the saturated magnetization M_S and the anisotropy constant K attributed to the 50-nm-thick $Fe_{65}Au_{35}$ layer. They exhibit a very flat temperature dependence in the 5–300 K temperature range, which is expected for a $Fe_{65}Au_{35}$ alloy with a Curie temperature around 700 K. The

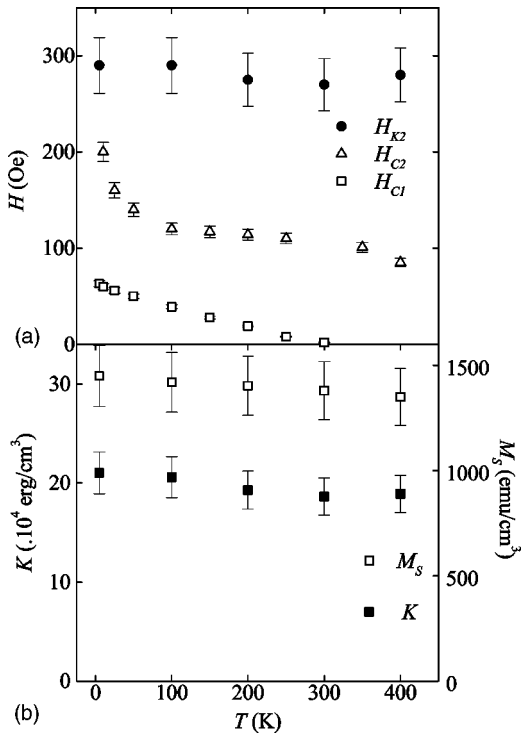

FIG. 5. Temperature (T) dependence on $Fe_{30}Au_{70}$ (100 nm)/Au (3 nm)/$Fe_{65}Au_{35}$ (50 nm) of (a) H_{C1}, the coercive field of $Fe_{30}Au_{70}$ layer (open square), H_{C2}, the coercive field of $Fe_{65}Au_{35}$ layer (open triangle), and H_{K2}, its anisotropy field (solid circle) and (b) M_S, the saturation magnetization (open square), and the anisotropy constant K (solid square) for the $Fe_{65}Au_{35}$ alloy.

influence of the $Fe_{65}Au_{35}$ layer thickness $t_{Fe_{65}Au_{35}}$ was studied for 30 nm$< t_{Fe_{65}Au_{35}} <$100 nm at $T=400$ K in coupled devices with a 100-nm-thick $Fe_{30}Au_{70}$ layer. M_S and H_{K2} were found to be independent of the $Fe_{65}Au_{35}$ layer thickness whereas H_{C2} was found to decrease from $H_{C2}=110$ Oe for $t_{Fe_{65}Au_{35}}=30$ nm to $H_{C2}=25$ Oe for $t_{Fe_{65}Au_{35}}=100$ nm.

From the parameters H_K, M_S, and T_C, we could evaluate the exchange integrals and anisotropy energy and finally the magnetic domain wall characteristics: energy and thickness in zero applied field. We followed the methods developed by previous authors using a mean-field method. They are not totally justified in systems that develop itinerant magnetism but provide nevertheless good orders of magnitude of the micromagnetics quantities. The exchange integral $J_{Fe\text{-}Fe}$ in the $Fe_xAu_{(1-x)}$ alloys has been estimated in the frame of the mean-field theory by $J_{Fe\text{-}Fe}=3\,k_BT_C/2\,z\,x\,S_{Fe}(S_{Fe}+1)$ where $T_C=350$ K for $x=0.3$ and 700 K for $x=0.65$, and z is the coordinence ($z=12$ for an fcc structure and $z=8$ for the bcc one). S_{Fe} has been evaluated from the moment per Fe atom: $\mu_{Fe}=g\,\mu_BS_{Fe}$ with $g=2.2$, which leads to $J_{Fe\text{-}Fe}=0.8\,10^{-14}$ erg and 1×10^{-14} erg for $x=0.3$ and 0.65, respectively. The exchange constant A' is then calculated with

$$A'(T)=\frac{nJ_{Fe\text{-}Fe}x^2}{a}\left(\frac{\mu_{Fe}(T)}{g\mu_B}\right)^2,$$

where a is the lattice parameter and $n=4$ for fcc structure and $n=2$ for the bcc one.[30] For $T=10$ K, the exchange stiffnesses for $Fe_{30}Au_{70}$ and $Fe_{65}Au_{35}$ were estimated, respectively, to 1×10^{-7} erg/cm^3 and 4.5×10^{-7} erg/cm^3. In the frame of a discontinuous linear chain of spins, the energy per surface unit, σ, and the domain walls thickness δ under zero field in each alloy have been deduced from $\delta=\pi\sqrt{2A'/K}$ and $\sigma=\pi\sqrt{2A'K}$. At 10 K we found $\delta=90$ nm and $\sigma=0.2$ erg/cm^2 for $Fe_{30}Au_{70}$ and $\delta=70$ nm and $\sigma=1.3$ erg/cm^2 for $Fe_{65}Au_{35}$. Beyond these values, we have to keep in mind that the domain wall widths are of the same order of magnitude in both alloys, but that the energy of a domain wall is about 6 times larger in $Fe_{65}Au_{35}$ than in $Fe_{30}Au_{70}$. This means that the interface between the two layers constitute a potential step from $Fe_{30}Au_{70}$ to $Fe_{65}Au_{35}$ that the domain wall will have to overcome to propagate from one layer to the other one. At $T=300$ K, the domain wall width and energy are estimated to be 37 nm and 0.05 erg/cm^2 in the $Fe_{30}Au_{70}$ alloy and 67 nm and 1.2 erg/cm^2 in $Fe_{65}Au_{35}$. The ratio between the domain wall energy in the two alloys is then increased from 6 at 5 K to about 25 at 300 K.

From the characteristics of the two layers, the $Fe_{30}Au_{70}/Fe_{65}Au_{35}$ bilayer appears to be a model system to study the pinning of a well-defined domain wall at the interface between the two layers since (1) both layers exhibit an uniaxial anisotropy, (2) a chemical continuity is maintained between the two layers, and (3) the domain wall energy is significantly larger in the $Fe_{65}Au_{35}$ system, so the $Fe_{30}Au_{70}/Fe_{65}Au_{35}$ bilayer is about to constitute a potential energy step for a domain wall previously created in the $Fe_{30}Au_{70}$ layer. Note that those characteristics make the $Fe_{30}Au_{70}/Fe_{65}Au_{35}$ bilayer a unique exchange-coupled system compared to other ''conventional'' spring magnet systems.[4,9–11,18,31]

III. MAGNETIC CONFIGURATIONS IN COUPLED LAYERS

A. Magnetization measurements

The typical magnetic behavior, with the field applied along the easy axis at $T=10$ K, of a $Fe_{30}Au_{70}$(100 nm)/$Fe_{65}Au_{35}$ (50 nm) system made of two coupled layers is shown in Fig. 6(b). It is compared to the behavior of the $Fe_{30}Au_{70}$(100 nm)/Au (3 nm)/$Fe_{65}Au_{35}$(50 nm) system made up of the two same layers but separated by a decoupling gold layer [Fig. 6(a)]. Four qualitative differences between the coupled and uncoupled systems are observed. (i) The amplitude of the first drop in the coupled system is reduced and is smaller than the one observed in the uncoupled system. It indicates that the reversal of the $Fe_{30}Au_{70}$ layer magnetization, which reverses first, is not complete. The field at which the reversal of the magnetization starts is close to the coercive field of the individual layer. Nevertheless, it will be called H_{R1} instead of H_{C1}. (ii) In the coupled system, the minor loop [Fig. 6(b)] is no longer centered about 0 but about a negative field H_E. (iii) In the intermediate stage, between the two magnetization steps and while going back

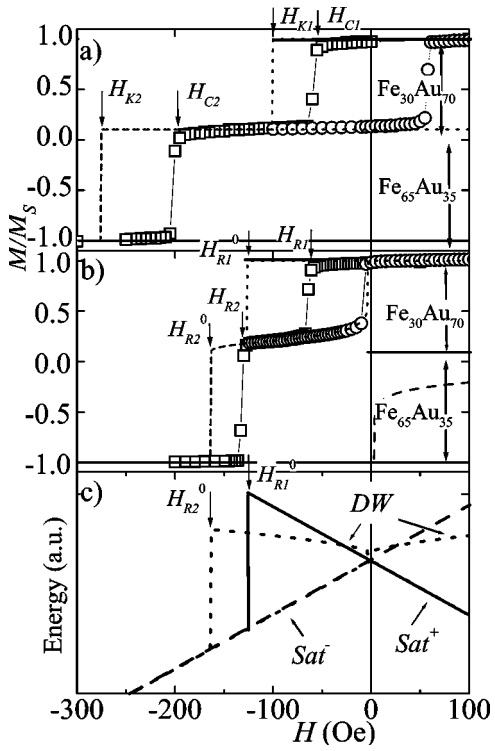

FIG. 6. (a) Experimental normalized magnetization (M/M_S) as a function of the field H applied along the easy axis obtained at 10 K on a $Fe_{30}Au_{70}$ (100 nm)/Au (3 nm)/$Fe_{65}Au_{35}$ (50 nm) layer for H swept from 500 Oe to -500 Oe (open square) and from 500 Oe to -120 Oe back to 500 Oe (open circle). H_{C1} and H_{C2} are, respectively, the measured coercive field of the $Fe_{30}Au_{70}$ layer and the $Fe_{65}Au_{35}$ layer. H_{K1} (H_{K2}) is the calculated field at which the $Fe_{30}Au_{70}$ layer ($Fe_{65}Au_{35}$ layer) magnetization can no longer be pointed along the positive field direction it is also its anisotropy field. Lines are the calculated M/M_S. (b) Experimental normalized magnetization (M/M_S) as a function of the field H applied along the easy axis obtained at 10 K on a $Fe_{30}Au_{70}$(100 nm)/$Fe_{65}Au_{35}$ (50 nm) layer for H swept from 500 Oe to -500 Oe (open square) and from 500 Oe to -120 Oe back to 500 Oe (open circle). H_{R1} and H_{R2} are, respectively, the measured field for which the $Fe_{30}Au_{70}$ layer and the $Fe_{65}Au_{35}$ layer magnetization reverse. Lines are the calculated M/M_S (solid lines correspond to sat^+ or sat^- states and dash line to the DW state). H_{R1}^0 and H_{R2}^0 are, respectively, the calculated field at which the sat^+ state and the DW state no longer exist. (c) Evolution of the energy of the three sates: sat^+ (solid line), sat^- (dashed line), and DW (dotted line) as a function of the applied field along the easy axis.

from $H_{R1}>H>H_{R2}$ to 0, the normalized magnetization shows a slope with respect to the field variation which is stronger in the coupled system than in the decoupled one. (iv) Finally, it occurs that the second step, which corresponds to the reversal of the $Fe_{65}Au_{35}$ layer magnetization, occurs at a field H_{R2} significantly smaller than H_{C2}.

All these facts show that the layers are actually coupled and interact with each other. The evolution of the magnetization is qualitatively consistent with a model, where the key role is played by an interface domain wall: starting from a saturated magnetization, there is first at H_{R1} a nucleation of the magnetization reversal in the softer layer $Fe_{30}Au_{70}$. The nucleation occurs from the outer surface of the layer and the reversal of the magnetization spreads through the layer. It is stopped at the interface between the two materials where a domain wall is trapped by the potential step due to the change of materials. At this stage, the domain wall can be compressed by increasing the field or decompressed by lowering it, which explain why this part of the magnetization curve (for $H_{R1}>H>H_{R2}$) is not flat and decreases when the amplitude of the field increases. Finally, while increasing the amplitude of the field, the domain wall becomes more and more compressed and under the pressure generated by the magnetic field, the magnetization of $Fe_{65}Au_{35}$ layer reverses at a field H_{R2} smaller than H_{C2}. The sample is acting as a domain wall junction. The domain wall (DW) junction is a model device proposed by Gunther and Barbara[32] to study the DW dynamic across an energy barrier. In this structure a DW may be trapped by a potential step, and as the field increases, because of the Zeeman energy, the potential step vanishes and the DW may move freely.

B. Micromagnetism calculation

In order to quantitatively characterize the evolution of magnetic configurations involved in exchange-coupled $Fe_{30}Au_{70}/Fe_{65}Au_{35}$ bilayers, energy minimum configurations were calculated considering the system as a spin chain. This modeling is very similar to the one used in Refs. 8 and 18. Each spin i has its own magnetization M_i, uniaxial anisotropy constant K_i, and is exchange coupled to its first-neighbor spins by an exchange stiffness $A_{i,i+1}$ and $A_{i-1,i}$. A magnetic field H is applied on the spin chain along the easy axis. The model is restricted to equilibrium in-plane configurations since the demagnetizing field tends to maintain the magnetization in the plane of the film. By integrating over the whole bilayer thickness t we obtained the energy per surface unit given by

$$E=\int_0^t\left[A\left(\frac{d\theta}{dz}\right)^2+K\sin^2\theta-H\cdot M\cos\theta\right]dz. \qquad (1)$$

To determine the possible energy minima, Eq. (1) was transformed into a discrete form (so that each spin describes a 1-nm-thick layer) and minimized. Several solutions corresponding to different local minima of energy were obtained using four different initial magnetic profiles: two saturated configurations, one with the magnetization pointing along the positive field direction (sat^+) and the other one along the negative field direction (sat^-) and two configurations with an antiparallel alignment of the two layers magnetization. The parameters (A, K, and M_S) used to perform the micromagnetic calculation are gathered in Table I and are found to be within the error bars of the parameters previously measured and calculated. The calculation should then permit us to determine which magnetic configurations are possible whereas magnetization measurements provide which configuration is actually adopted at a given temperature.

The calculation was first tested in the case of the uncoupled layer [Fig. 6(a)] and the results are found to be in accordance with the Stoner-Wholfart model:[28] the $Fe_{30}Au_{70}$

TABLE I. Magnetic parameters A (exchange stiffness), K (anisotropy constant), and M_S (saturation magnetization) for $Fe_{30}Au_{70}$ alloy layer and $Fe_{65}Au_{35}$ alloy layer used to perform the micromagnetic calculation. The interface exchange stiffness was estimated to 3×10^{-7} erg/cm.

$T=5$ K	M_S (emu)	A (erg/cm)	K (erg/cm^3)
$Fe_{30}Au_{70}$	550	1×10^{-7}	2.75×10^4
$Fe_{65}Au_{35}$	1350	4.5×10^{-7}	20×10^4

($Fe_{65}Au_{35}$) magnetization may be pointing antiparallel to the field as long as $H>H_{K1}$ (H_{K2}). For $H=H_{K1}$ (or H_{K2}), the energy barrier between the parallel and antiparallel states vanishes. However, during an experiment at a given temperature, the magnetization may switch from an antiparallel to a parallel state for an applied field $H>H_{K1}$ by crossing the energy barrier between the two states.

For coupled layers the field dependence of the calculated energy minimum solution [Fig. 6(c)] and the resulting magnetization component parallel to the field [Fig. 6(b)] are evaluated. For all fields, very good agreement is found between the measured magnetization and calculated magnetizations of one of the energy minimum solution. This permits us to give a quantitative interpretation of the magnetization versus field measurements performed on the coupled layer.

Starting from a large positive field the only energy minimum is the one for which all the spins are pointing along the field direction and parallel to the easy axis (the sample is saturated). For such a positive field, all energy terms, anisotropy, exchange coupling inside the layers, and at the interface, and Zeeman energy are minimum, the sample magnetization is kept in the saturated configuration along the cooling direction (sat^+). The energy of the configuration sat^+ exhibits a linear dependence with the field because only the Zeeman energy terms varies [Fig. 6(c)]. While decreasing the magnetic field, the Zeeman energy becomes smaller and two metastable minima appear successively: one with all moments opposite to the field (sat^-) and a second one (DW) with a domain wall located at the bilayer interface. For $H>0$, coming from the sat^+ configuration, the system has no reason to leave this configuration to a higher-energy minimum.

When crossing the zero field, the energy of sat^+ and sat^- are reversed and the sat^- state becomes the more stable one. The energy of the DW state is higher than sat^+ and sat^- for fields near $H=0$ because of the contribution of exchange and anisotropy in the DW. When increasing the field in the negative direction, sat^+ is less and less stable, and according to our calculation, its local minimum disappears near $H_{R1}^0\approx-125$ Oe. For this field, the energy barrier between the sat^+ and DW states vanishes. It means that the system will necessarily have left the sat^+ configuration beyond -125 Oe to reach either the more stable sat^- state or the intermediate DW configuration. If it reaches the DW configuration, it has to leave it beyond $H_{R2}^0\approx-165$ Oe to sat^-, for which the barrier between DW and sat^- vanishes.

From magnetization measurements it is clear that at H_{R1} the system drops first from the sat^+ state to the DW state and before $H_{R1}^0\approx-125$ Oe. Then it drops from DW to sat^- before $H_{R2}^0\approx-165$ Oe, which means that the activation energy should play a key role in the transition. A remarkable feature is that the experimental amplitude of the net magnetization drop at H_{R1} is very close to the difference between the magnetization calculated in the sat^+ and DW states at this field. On the other hand, the experimental variation of the magnetization in the DW state follows the calculated one. This means that the model of compression and decompression of the domain wall is perfectly justified. The calculated profiles of the domain wall submitted to three different fields are shown in Fig. 7. It can be noticed that at low field ($H=15$ Oe) the DW thickness obtained from numerical calculations reaches the order of magnitude of the DW thickness calculated in zero field from $\delta=\pi\sqrt{2A'/K}$. Furthermore, the decrease of the DW thickness as the applied field increases is clearly visible. Note that the DW spreads mainly in the $Fe_{30}Au_{70}$ but penetrates also slightly into the $Fe_{65}Au_{35}$ layer, which is consistent with the fact that the ratio between the energies of the domain wall in these two alloys is moderate (~6).

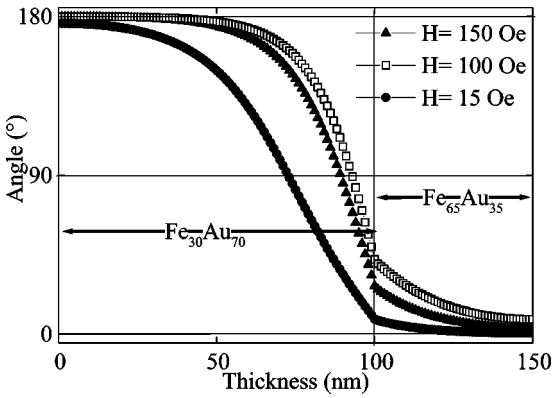

FIG. 7. Magnetic configuration for three different fields H applied along the easy axis ($H=15$ Oe, $H=100$ Oe, $H=150$ Oe) obtained by plotting the angle between the magnetic moment and the positive field direction vs the position of the considered magnetic moment in the bilayer thickness.

The calculation permits us to know which states are possible but not at which field those states are reached. For instance concerning the reversal from the DW state to the sat^- state, the simulation predicts that this last configuration is always energetically favorable and that for $H=-165$ Oe the DW state can no longer exist since this energy well is longer more present (in other words, the energy barrier has vanished). The question as to why the magnetic configuration of the system changes before the energy barrier vanishes is discussed in Sec. V.

C. Thickness dependence

A detailed study of the effects of the parameters of the system on the magnetization reversal process was performed. We focused especially on the thickness of the layers (t_1 for the Fe_{65} Au_{35} layer and t_2 for the $Fe_{30}Au_{70}$ layer). The effect of t_1 is shown in Fig. 8 where the magnetic behaviors of

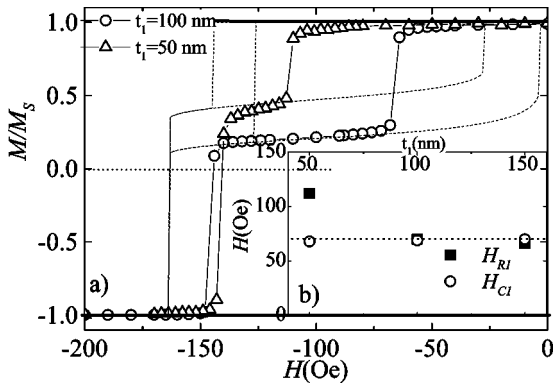

FIG. 8. (a) Experimental normalized magnetization (M/M_S) as a function of the field H applied along the easy axis obtained at 10 K on a $Fe_{30}Au_{70}$ (100 nm)/$Fe_{65}Au_{35}$ (50 nm) bilayer (open circle) and obtained on a $Fe_{30}Au_{70}$ (50 nm)/$Fe_{65}Au_{35}$ (50 nm) bilayer (open triangle). Lines are the calculated M/M_S (solid lines correspond to sat^+ or sat^- states and dashed line to the DW state). (b) Thickness (t_1) dependence of H_{C1}, the coercive field of a $Fe_{30}Au_{70}$ (t_1 nm), and H_{R1}, the field at which the $Fe_{30}Au_{70}$ layer magnetization reverses in a $Fe_{30}Au_{70}$ (t_1 nm)/$Fe_{65}Au_{35}$ (50 nm) bilayer.

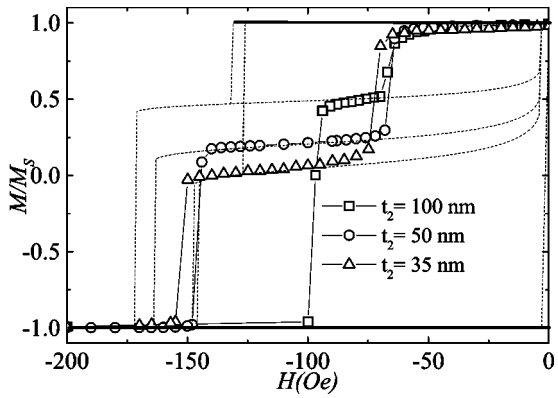

FIG. 9. Normalized magnetization (M/M_S) as a function of the field H applied along the easy axis obtained at 10 K on a $Fe_{30}Au_{70}$ (100 nm)/$Fe_{65}Au_{35}$ (t_2 nm) layer for $t_2=100$, 50, and 35 nm. Lines are the calculated M/M_S (solid lines correspond to sat^+ or sat^- states and dash line to the DW state).

$Fe_{30}Au_{70}$(100 nm)/$Fe_{65}Au_{35}$(50 nm) and $Fe_{30}Au_{70}$(50 nm)/$Fe_{65}Au_{35}$(50 nm) are compared. It occurs that H_{R1} increases when t_1 decreases which shows that the nucleation of the magnetization reversal is more difficult for lower t_1 thickness. This is also confirmed by a numerical calculation that shows that the energy well for the DW state appears and the energy barrier between sat+ and DW vanishes for larger field when t_1 decreases (H^0_{R1} increases as t_1 decreases). As magnetization reversal of the $Fe_{30}Au_{70}$ layer requires the formation of an interface domain wall, it can be imagined that H_{R1} will be shifted from H_{C1} as soon as the thickness of the $Fe_{30}Au_{70}$ layer is smaller than the width of the domain wall, which means no ''free'' domain wall can be created. The inset of Fig. 8 shows that at 10 K for $t_1=100$ nm and 150 nm, H_{R1} is very close to H_{C1} and that for $t_1=50$ nm it is significantly shifted, which is consistent with Table I which reports that the expected domain wall thickness for a $Fe_{30}Au_{70}$ alloy is close to 90 nm at 10 K. However, H_{R2} is not significantly affected by the t_1 variation.

The effect of t_2, the $Fe_{65}Au_{35}$ layer thickness, is shown in Fig. 9. H_{R2} is found to be reduced as t_2 increases. This behavior is probably correlated to intrinsic effects of the layer and has to be related to the decrease of the $Fe_{65}Au_{35}$ coercive field as its thickness decreases. Magnetizations deduced from the simulations are well superimposed with the experimental points when the DW is present. Unlike the field H_{R2} deduced from experimental measurements, H^0_{R2} is found to increase as the thickness t_2 is increased.

IV. EVIDENCE OF THE TRANSVERSE MAGNETIZATION COMPONENT OF THE DOMAIN WALL

If in the saturated state all magnetic moments are along the field direction, parallel or antiparallel to it, the domain wall state is characterized by a distribution of orientation of the magnetic moments which have to exhibit components perpendicular to the field direction. The extreme case is that of spins located in the middle of the domain wall which are orientated perpendicularly to the field (in the plane of the sample). As the transverse component of the spin is not detected by the magnetization measurements the presence of DW had to be revealed by indirect techniques. We present here evidences from magnetic susceptibility and resistivity measurements.

A. Magnetic susceptibility

The response of a ferromagnetic system to an alternative magnetic field is mainly due to the transverse component of the magnetization. The longitudinal response lowers rapidly to 0 below the Curie temperature and as a consequence, the ac susceptibility is a measurement of the ''quantity'' of the magnetic moment perpendicular to the field. In our experiments, the ac susceptibility was collected by superposing a 1000-Hz ac field of 2 Oe onto the static field. The data collected in the static field range $+200-200$ Oe are plotted in Fig. 10 with the quasistatic magnetization results. The sharp susceptibility steps for H_{R1} and H_{R2} correspond to an abrupt increase or decrease of the spin population exhibiting a component perpendicular to the magnetic field. They precisely occur at fields H_{R1} (up) and H_{R2} (down) which have been identified as the fields at which the domain wall were created and annihilated. These transitions support the hypothesis of a domain wall formation, imagined from the amplitude of the static magnetic transition and already supported by the numerical simulations. The progressive decrease of the magnetic susceptibility between H_{R1} and H_{R2} is then consistent with the compression of the domain wall as calculated (Fig. 7): as the domain wall thickness decreases the number of spins having a component perpendicular to the ac field lowers and so does the ac-susceptibility signal.

B. Magnetoresistance

The magnetoresistance anisotropy effect constitutes a second piece of evidence of the occurrence of the domain wall

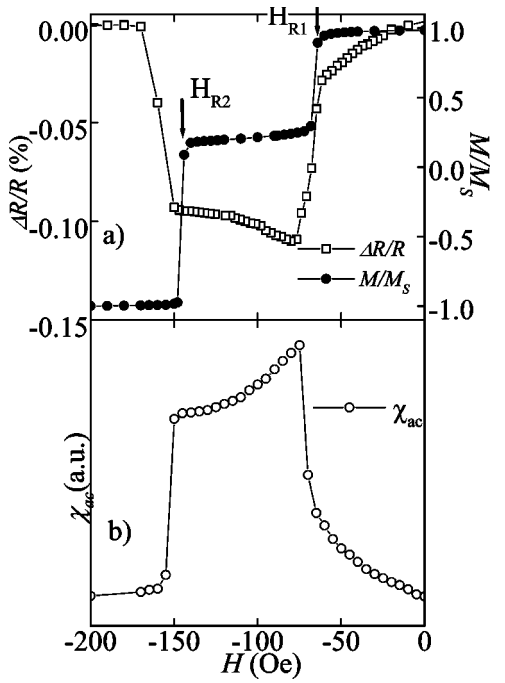

FIG. 10. (a) Normalized magnetization (M/M_S) and magnetoresistance ($\Delta R/R$) as a function of the magnetic field H applied along the easy axis measured at 10 K on a $Fe_{30}Au_{70}$(100 nm)/$Fe_{65}Au_{35}$ (50 nm) bilayer. (b) ac susceptibility vs H measured on a $Fe_{30}Au_{70}$ (100 nm)/$Fe_{65}Au_{35}$ (50 nm) bilayer at 10 K.

through the transverse magnetic component of the spins. In iron-based samples, this effect manifests itself by a maximum of electrical resitivity when the electrical current travels along the direction of the magnetic moments (parallel or antiparallel) and by a minimum of resistivity when it travels perpendicularly to them.[8,18] As shown in Fig. 10(a), the electrical resistivity with the electrical current along the magnetic field exhibits two down and up steps at H_{R1} and H_{R2} corresponding to the creation and disappearance of the domain wall, respectively. These transitions are unambiguously due to the successive appearance and disappearance of the transverse component of the magnetic moment. In a similar way as for the susceptibility, the increase of the resistivity between H_{R1} and H_{R2} is due to the compression of the domain wall. Finally, we can notice that the resistivity decreases slowly from $H=0$ Oe to H_{R1}, which may be explained by the occurrence of a transverse magnetization component preceding the nucleation of the magnetization reversal in the $Fe_{30}Au_{70}$ layer. Note that this last phenomenon is not detected by the magnetization measurements but could be noticed using ac-susceptibility measurements [Fig. 10(b)].

V. DYNAMIC OF MAGNETIZATION REVERSAL IN COUPLED LAYERS

A. Temperature dependence

It turned out that the magnetic behavior of the coupled system is strongly temperature dependent and that, in a large extent, two thermal effects mix: (i) the temperature activates the crossing of energy barrier by the domain wall and (ii) the temperature modifies the magnetic characteristics (saturation magnetization, anisotropy) of the individual layers and as a consequence the heights of the barriers themselves.

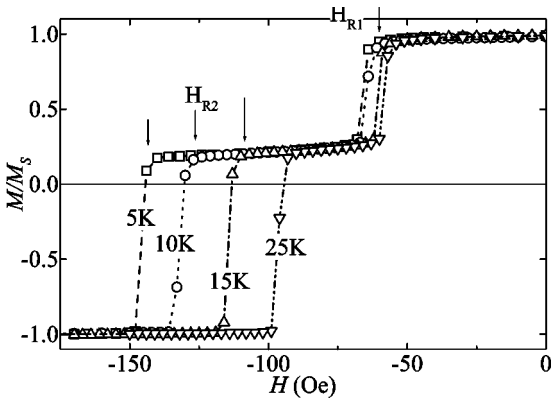

FIG. 11. Normalized magnetization (M/M_S) as a function of the magnetic field (H) applied along the easy axis of a $Fe_{30}Au_{70}$ (100 nm)/$Fe_{65}Au_{35}$ (50 nm) bilayer for different temperatures ranging from 5 to 25 K.

The two sets of magnetization curves pictured in Figs. 11 and 12 as well as the evolution of H_{C1}; H_{R1} and H_{R2} fields gathered in Fig. 13 illustrate these effects. Figure 11 which presents magnetization data collected from the $Fe_{30}Au_{70}$(100 nm)/$Fe_{65}Au_{35}$(50 nm) sample at low temperature exhibits typically what can be expected from a system in which the thermal activation process is dominant. In this restricted temperature range, far from T_C and where the magnetic parameters of the layers are very little temperature dependent, H_{R2} is strongly temperature dependent. The shift of H_{R2} towards low field has been observed in the GdFe/TbFe system and indicates that the crossing of the potential step is thermally activated. The nucleation of the domain wall at H_{R1} in $Fe_{30}Au_{70}$ decreases very slowly when increasing the temperature, which means it is slightly activated too.

Figure 12 shows the magnetization data collected in a wide temperature range for $T=150$ K, 300, and 350 K. At 350 K, there is only one magnetization step left which corresponds to the coercive field of a unique $Fe_{30}Au_{70}$ (100 nm) layer. It is consistent with the fact that the $Fe_{30}Au_{70}$ is above its T_C and as a consequence the $Fe_{65}Au_{35}$ layer is magneti-

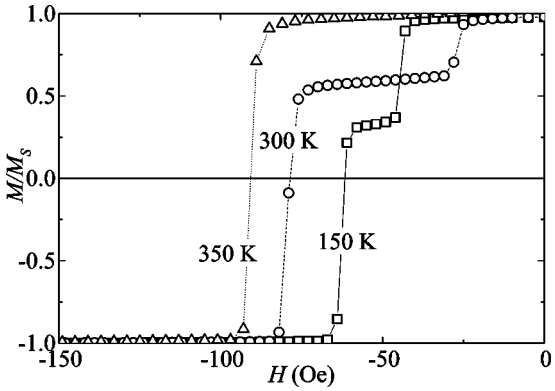

FIG. 12. Normalized magnetization (M/M_S) as a function of the magnetic field (H) applied along the easy axis of a $Fe_{30}Au_{70}$ (100 nm)/$Fe_{65}Au_{35}$ (50 nm) bilayer for different temperatures ranging from 150 to 350 K.

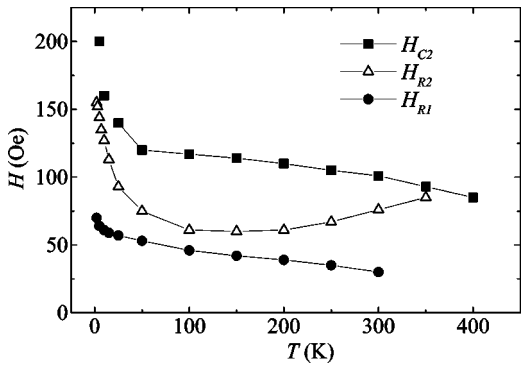

FIG. 13. Temperature dependence of H_{C1}, the coercive field of the $Fe_{30}Au_{70}$ (100 nm) layer, H_{C2}, the coercive field of the $Fe_{65}Au_{35}$ (50 nm) layer, and H_{R2}, the field at which the system $Fe_{30}Au_{70}$ (100 nm)/$Fe_{65}Au_{35}$ (50 nm) switches from the DW state to the sat state.

cally uncoupled. The magnetization curves collected below the Curie temperature of $Fe_{30}Au_{70}$ exhibit the transitions at H_{R1} and H_{R2} (see $T=150$ K and $T=300$ K) which means that at these temperatures blocking of the domain wall still exists. However, H_{R2} goes through a minimum near $T=120$ K, which means that above this temperature, and probably well below, the height of the barrier is strongly temperature dependent and the thermal activation cannot be isolated.

B. After effect measurements

In order to study the activation process involved in the FeAu magnetization layer reversal and so the crossing from a DW state to a sat state, we limited our temperature range to the 3–10 K, in which magnetic parameters can be considered as constant. As shown in Fig. 14, H_{R2} depends strongly on the temperature, and as explained above, this change cannot be attributed to the thermal dependence of the magnetic parameters. Relaxation measurements were performed with the following procedure: at each temperature appearing in Fig. 14, the system was brought to a set of fields close to H_{R2},

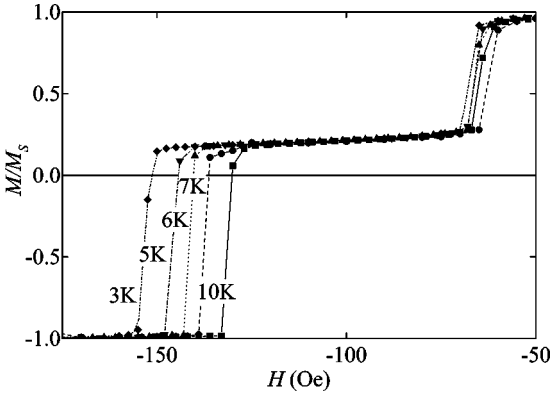

FIG. 14. Normalized magnetization (M/M_S) as a function of the magnetic field (H) applied along the easy axis of a $Fe_{30}Au_{70}$ (100 nm)/$Fe_{65}Au_{35}$ (50 nm) bilayer for different temperatures (3, 5, 6, 7, and 10 K).

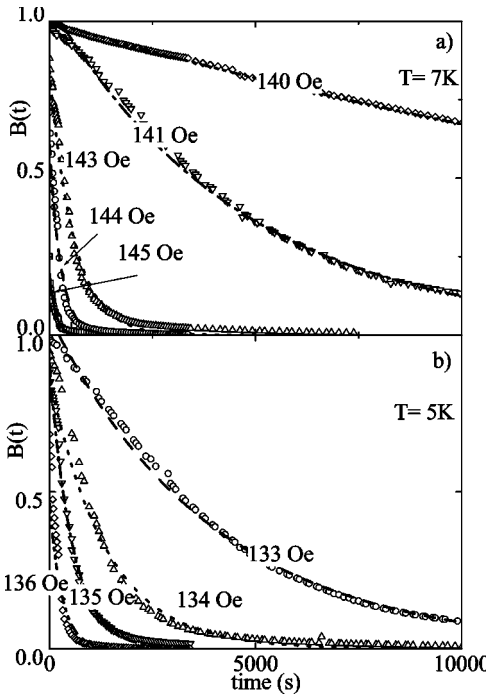

FIG. 15. Reduced magnetization $B(t)=[M(t)-M_{DW}]/[M_{DW}-M_{Sat-}]$ as a function of time (t) for different applied magnetic fields at (a) 7 K and (b) 5 K.

and then under constant field, isothermal measurements of the magnetization $M(t)$ were performed as a function of time.

From $M(t)$, we introduced the reduced $B(t)$ parameter, defined by

$$B(t)=\frac{M(t)-M_{DW}}{M_{DW}-M_{Sat-}}, \tag{2}$$

where M_{DW} is the magnetization in the DW state before the magnetization drop and M_{Sat-} is the magnetization in the saturated state. $B(t)$ represents the fraction of the average magnetization that has not reversed. Two set of examples of the time evolution of $B(t)$ are shown in Figs. 15(a) and 15(b) for $T=5$ K and 7 K respectively. All the $B(t)$ curves may be fitted by an exponential decay with a single relaxation time τ:

$$B(t)=B_0\exp\left(\frac{-t}{\tau(H,T)}\right), \tag{3}$$

where B_0 is the value of B for $t=0$.

This expression (3) would be consistent with a model of sample made of a large number of identical and independent magnetic domains (single relaxation time τ) in which a DW is pinned by an energy barrier. That hypothesis implies that a domain switching from a DW state to a sat state is the only reversal process. This description is consistent with exponential decay observed on the magnetization versus time plot.[33] However, we should keep in mind that domain growing is not taken into account in this model. The above domains could then defined as domains wall junctions (DWJ's) as proposed by Gunther and Barbara.[32] A DWJ is a magnetic

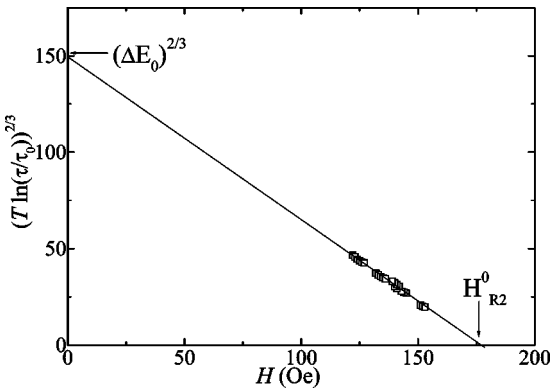

FIG. 16. Field (H) dependence of $[T\ln(\pi/\tau_0)]^{2/3}$. For the linear dependence, ΔE_0 can be estimated to 1800 K and H^0_{R2} to 175 Oe.

nanostructure inside which a DW feels a potential energy barrier. The probability $P(t)$ for each DW to cross the barrier before time t is then given by:

$$P(t)=1-\exp\left(\frac{-t}{\tau(H,T)}\right), \tag{4}$$

where $\tau(H,T)$ is the relaxation time. Following the analysis of Gunther and Barbara on the field dependence of the height of the energy barrier seen by a DW,

$$\tau(H,T)=\tau_0\exp\left(\frac{\Delta E(H)}{kT}\right), \quad \Delta E(H)=\Delta E_0\left(1-\frac{H}{H^0_{R2}}\right)^{\alpha}, \tag{5}$$

where ΔE_0 is the energy barrier height in zero field, $\tau_0=1/\Gamma_0$ where Γ_0 is the attempt frequency, and $\alpha=3/2$ when $\varepsilon=(1-H/H^0_{R2})\ll 1$. Also in this model H^0_{R2} is the field at which the barrier vanishes because the positive slope of the interface potential is compensated by the negative slope of the Zeeman energy. τ_0 could be estimated from the relation

$$\tau_0=\tau_1\exp\left[\frac{-T_2}{T_2-T_1}\ln\left(\frac{\tau_1}{\tau_2}\right)\right],$$

which requires two experiments performed at the same field but at different temperatures. This condition is not easy to fulfill; however, from τ_1 (6 K,142 Oe)$=115$ s and τ_2 (5 K,142 Oe)$=49\,000$ s, τ_0 could be estimated to 10^{-10} s. This value is in fact supported by a global analysis of the data based on the fact that for a same sample, the curve in Fig. 16 showing $[T\ln(\pi/\tau_0)]^{2/3}$ versus H must be continuous over the different measurement temperatures, independently of the relation between ΔE and H (Ref. 31).

From this curve, ΔE_0 can be estimated to 1800 K and H^0_{R2} to 175 ± 10 Oe; this value lies within the hypothesis for the use of the model of Gunther and Barbara: $\varepsilon=(1-H/H^0_{R2})\leqslant 0.3<1$. The fact that by two different methods the same value of H^0_{R2} has been obtained gives even more credit to the DWJ theory. Indeed the micromagnetic calculation predicts the vanishing of the metastability of the domain wall for $H^0_{R2}=165$ Oe.

The above authors described a different DWJ class depending on the characteristic DWJ length (layer thickness, energy barrier width, etc.) compared to the domain wall thickness. It then has to be pointed out that $Fe_{30}Au_{70}$(100 nm)/$Fe_{65}Au_{35}$(50 nm) is a new class of DWJ since the thickness of the magnetic layer which is the cause of the energy barrier is comparable of the domain wall width, whereas in the case of GdFe/TbFe/GdFe DWJ, the TbFe layer thickness was very thin (0.2–2 nm) compared to the DW thickness in the GdFe layer (50 nm) (Ref. 31).

VI. CONCLUSION

For $Fe_{30}Au_{70}/Fe_{65}Au_{35}$ bilayers, specific growth conditions allow us to induce a uniaxial anisotropy in both ferromagnetic alloys. Precise characterizations of their magnetic properties have shown that the bilayer can be classified as a ''spring magnet.'' The ferromagnetic layers are ferromagnetically exchange coupled at the interface and the domain wall energy is significantly different from one layer to the other: this ratio is evaluated to about 6 at low temperature. However, this difference is moderate compared to other spring magnet systems.[1,3,7–9,11] When a magnetic field is swept along the easy axis, magnetization reversal from one saturated state to the other occurs via an interface domain wall state which is metastable. Because of the moderate domain wall energy ratio, this interface domain wall is present in both layers. However, it spreads mainly in the soft $Fe_{30}Au_{70}$ layer and is pinned and compressed by the field against the harder $Fe_{65}Au_{35}$ layer. Its presence and its compression are evidenced by magnetization measurements combined with micromagnetic calculation and using transport and ac-susceptibility measurements. Both of these techniques are found to be very sensitive to the presence of a magnetization component perpendicular to the applied field and consequently to the domain wall. The system can reach its minimum saturated state when the domain wall overcomes the energy barrier. In order to characterize this barrier, the temperature dependence as well as magnetic aftereffect measurements has been performed. The magnetization reversal process was found to be thermally activated and activation parameters could be deduced. The field for which the energy barrier vanishes is found to be very close to the one deduced from simulations using the magnetic characteristics of individual layers. This result allows us to assert that the energy barrier felt by the DW is due to the specific magnetic properties of the alloys and that the $Fe_{30}Au_{70}/Fe_{65}Au_{35}$ device can be considered as a model system of domain wall junctions.

*Corresponding author. Electronic address: mangins@lpm.u-nancy.fr

[1] E.E. Fullerton, J.S. Jiang, M. Grimsditch, C.H. Sowers, and S.D. Bader, Phys. Rev. B **58**, 12 193 (1998).

[2] S. Wuchner, J.C. Toussaint, and J. Voiron, Phys. Rev. B **55**, 11 576 (1997).

[3] S. Mangin, G. Marchal, and B. Barbara, Phys. Rev. Lett. **82**, 4336 (1999).

[4] A.E. Berkowitz and K. Takano, J. Magn. Magn. Mater. **200**, 552 (1999).
[5] J. Nogues and I.K. Schuller, J. Magn. Magn. Mater. **192**, 203 (1999).
[6] Miguel Kiwi, J. Magn. Magn. Mater. **234**, 584 (2001).
[7] E. Goto, N. Hayashi, T. Miyashita, and K. Nakagawa, J. Appl. Phys. **36**, 2951 (1965).
[8] Y. Suzuki, R.B. Van Dover, E.M. Gyorgy, J.M. Phillips, and R.J. Felder, Phys. Rev. B **53**, 14 016 (1996).
[9] Z.J. Guo, J.S. Jiang, J.E. Pearson, S.D. Bader, and J.P. Liu, Appl. Phys. Lett. **81**, 2029 (2002).
[10] K. Mibu, T. Nagahama, T. Shinjo, and T. Ono, Phys. Rev. B **58**, 6442 (1998); K. Mibu, T. Nagahama, and T. Shinjo, J. Magn. Magn. Mater. **163**, 75 (1996).
[11] D. Chumakov, R. Schafer, D. Elefant, D. Eckert, L. Schultz, S.S. Yan, and J.A. Barnard, Phys. Rev. B **66**, 134409 (2002).
[12] V.K. Vlasko-Vlasov, U. Welp, J.S. Jiang, D.J. Miller, G.W. Crabtree, and S.D. Bader, Phys. Rev. Lett. **86**, 4386 (2001).
[13] J. Nogues, D. Lederman, T.J. Moran, and Ivan K. Schuller, Phys. Rev. Lett. **76**, 4624 (1996).
[14] J. Nogues, C. Leighton, and Ivan K. Schuller, Phys. Rev. B **61**, 1315 (2000).
[15] S. Mangin, F. Montaigne, and A. Schuhl, Phys. Rev. B **68**, 140404(R) (2003).
[16] J.R. Childress *et al.*, IEEE Trans. Magn. **37**, 1745 (2001).
[17] B. Dieny, V.S. Speriosu, S.S.P. Parkin, J.C. Scott, B.A. Gurney, D.R. Wilhoit, and D. Mauri, Phys. Rev. B **43**, 1297 (1991).
[18] F. Montaigne, S. Mangin, and Y. Henry, Phys. Rev. B **67**, 144412 (2003).
[19] D. Mauri, H.C. Siegmann, P.S. Bagus, and E. Kay, J. Appl. Phys. **62**, 3047 (1987).
[20] N.C. Koon, Phys. Rev. Lett. **78**, 4865 (1997).
[21] M. Kiwi, J. Mejia-Lopez, R.D. Portugal, and R. Ramirez, Europhys. Lett. **48**, 573 (1999).
[22] R.L. Stamps, J. Magn. Magn. Mater. **242–245**, 139 (2002).
[23] S. Mangin, C. Bellouard, G. Marchal, and B. Barbara, J. Magn. Magn. Mater. **165**, 161 (1997).
[24] A.P. Maloemoff, J. Appl. Phys. **63**, 3874 (1988).
[25] S. Mader, A.S. Nowick, and H. Widmer, Acta Metall. **15**, 203 (1967).
[26] G. Marchal, Ph. Mangin, and Chr. Janot, Thin Solid Films **23**, S17 (1974).
[27] G. Marchal, Ph. Mangin, and Chr. Janot, Philos. Mag. **32**, 1007 (1975).
[28] E.C. Stoner and E.P. Wohlfarth, Philos. Trans. R. Soc. London, Ser. A **240**, 599 (1948).
[29] B.V.B. Sarkissian, J. Phys. F: Met. Phys. **11**, 2191 (1981).
[30] C.W. Chen, *Magnetism and Metallurgy of Soft Magnetic Material* (Dover, New York, 1986).
[31] S. Mangin, G. Marchal, C. Bellouard, W. Wernsdorfer, and B. Barbara, Phys. Rev. B **58**, 2748 (1998).
[32] L. Gunther and B. Barbara, Phys. Rev. B **49**, 3926 (1994).
[33] M. Labrune, S. Andrieu, F. Rio, and P. Bernstein, J. Magn. Magn. Mater. **80**, 211 (1989).